batteries

MDPI

Article

Multiband Multisine Excitation Signal for Online Impedance Spectroscopy of Battery Cells

Roberta Ramilli [1,*], Nicola Lowenthal [1], Marco Crescentini [1,2] and Pier Andrea Traverso [1]

[1] Department of Electrical, Electronic, and Information Engineering (DEI), University of Bologna, 40136 Bologna, Italy; nicola.lowenthal2@unibo.it (N.L.); m.crescentini@unibo.it (M.C.); pierandrea.traverso@unibo.it (P.A.T.)
[2] Advanced Research Center on Electronic Systems (ARCES), University of Bologna, 40123 Bologna, Italy
* Correspondence: roberta.ramilli@unibo.it

Abstract: Multisine electrochemical impedance spectroscopy (EIS) represents a highly promising technique for the online characterization of battery functional states, offering the potential to monitor, in real-time, key degradation phenomena such as aging, internal resistance variation, and state of health (SoH) evolution. However, its widespread adoption in embedded systems is currently limited by the need to balance measurement accuracy with strict energy constraints and the requirement for short acquisition times. This work proposes a novel broadband EIS approach based on a multiband multisine excitation strategy in which the excitation signal spectrum is divided into multiple sub-bands that are sequentially explored. This enables the available energy to be concentrated on a limited portion of the spectrum at a time, thereby significantly improving the signal-to-noise ratio (SNR) without substantially increasing the total measurement time. The result is a more energy-efficient method that maintains high diagnostic precision. We further investigated the optimal design of these multiband multisine sequences, taking into account realistic constraints imposed by the sensing hardware such as limitations in excitation amplitude and noise level. The effectiveness of the proposed method was demonstrated within a comprehensive simulation framework implementing a complete impedance measurement system. Compared with conventional excitation techniques (i.e., the sine sweep and the classical single-band multisine methods), the proposed strategy is an optimal trade-off solution both in terms of energy efficiency and measurement time. Therefore, the technique is a valuable solution for real-time, embedded, and in situ battery diagnostics, with direct implications for the development of intelligent battery management systems (BMS), predictive maintenance, and enhanced safety in energy storage applications.

Keywords: EIS; online impedance spectroscopy; lithium-ion batteries; multisine excitation; multiband; signal-to-noise ratio; BMS

Academic Editor: Xianglin Li

Received: 24 March 2025
Revised: 23 April 2025
Accepted: 4 May 2025
Published: 10 May 2025

Citation: Ramilli, R.; Lowenthal, N.; Crescentini, M.; Traverso, P.A. Multiband Multisine Excitation Signal for Online Impedance Spectroscopy of Battery Cells. *Batteries* **2025**, *11*, 188. https://doi.org/10.3390/batteries11050188

1. Introduction

Electrochemical impedance spectroscopy (EIS) has been proven to be a valuable tool for the characterization of the battery functional state. EIS data can be used for extracting equivalent circuit models (ECMs) of the battery [1,2], inferring state parameters as the rate capacity, the state of charge (SoC) and the state of health (SoH) [3,4], and predicting the degradation and thermal runaway [5,6]. In recent years, some progress has been made to adapt and integrate EIS-based techniques into battery management systems (BMSs) for the online monitoring of large battery packs [7,8], such as those used in electrical vehicles, but may also be a powerful method for the online monitoring and diagnosis at the

cell-level [9–11]. This would enable a much more precise monitoring of the real behavior of the whole battery pack, allowing for the implementation of smart functionalities that can lead to a more reliable battery system [12,13]. For this reason, online EIS has attracted interest from the research and technical community [14–16].

The most efficient method to directly estimate and analyze the impedance of a battery is by exciting it with a specially designed excitation signal in conjunction with a dedicated processing algorithm to improve the signal-to-noise ratio (SNR) and measurement quality. In particular, the type of excitation signal has been the subject of several investigations in order to both improve the impedance measurement accuracy and account for the measurement constraints given by the concept of the impedance of an electrochemical system. Indeed, the underlying assumption at the basis of EIS techniques is that the observed electrochemical system can be considered as a causal, linear time-invariant (LTI) system. For batteries, this requirement is valid only under specific conditions. Linear behavior can be assumed only when considering an appropriately small excitation amplitude, trading off with the SNR, while the prerequisite of stationarity is usually assured in offline EIS measurements but can only be fulfilled in online EIS measurements by shortening the total measurement time needed for a complete spectrum estimate in the bandwidth of interest, in order to meet the assumption of negligible time-variance of the battery during the measurement time. In addition, a fast online measurement is also necessary to have an adequate sampling rate of the evolution of the state of the battery cell (i.e., its SoC and SoH).

Excitation signals in impedance spectroscopy are divided into two main groups: the stepped frequency sweep (or narrowband excitation) and the broadband signals. Stepped frequency sweep is considered, to date, as the reference method in impedance spectroscopy and is blindly accepted when high accuracy is required [17]. However, it suffers from a very long measurement time as the selected frequencies are applied sequentially, making it impractical in online EIS. On the contrary, broadband signals are designed to contain multiple superimposed sine waves, each at a different frequency, to perform simultaneous excitation throughout the bandwidth and minimize the measurement time [18].

The most common broadband signals used for EIS are multisine signals and pseudo-random binary sequences (PRBSs). The multisine signal excites a selected limited number of frequency bins and allows for the highest degree of customization in terms of the number of parameters of the signal that can be controlled, thus the following analysis was focused on this kind of excitation. In the design of a multisine excitation signal, there is an inherent trade-off between the number of excited frequency points in the spectrum, the available power that limits the excitation amplitude, and the required SNR for accurate impedance measurements. Many works have discussed this problem [19–21].

This paper faced this trade-off by proposing an efficient version of a multisine excitation signal based on a “sub-band division” technique. More precisely, the division in sub-bands of the overall excitation spectrum allows for the maximum power available from the source to be concentrated, at each measurement step, within a smaller band with respect to the total bandwidth investigated, thus achieving a higher SNR on each tone while preserving fast measurement times. The proposed multiband multisine excitation is a novel and effective approach that balances between fast measurement and high accuracy, which are essential key performance indicators for online battery impedance spectrum diagnosis. This method has the potential to enhance the accuracy of online EIS-based systems without requiring substantial changes to existing hardware and takes approximately the same measurement time.

The rest of this article is organized as follows. Section 2 discusses the challenges of designing multisine excitation signals for impedance spectroscopy applied to battery cell monitoring. Section 3 describes the proposed multiband multisine approach and how

it represents a satisfactory trade-off between the measurement time and accuracy while Section 4 explains how to design a multiband multisine sequence in light of the system constraints, together with the simulations. Finally, the preliminary results are presented in Section 5, where the proposed strategy is applied for the acquisition of the impedance spectrum of a battery cell by simulating an EIS-based measurement system. Conclusions are drawn in Section 6.

2. Multisine Excitation Signal for EIS

2.1. Linearity and Stationarity Criteria

The definition of the impedance concept for an electrochemical system is possible only if the system meets the requirements of linearity and stationarity [22]. However, batteries are (i) inherently nonlinear due to the nonlinearity effects associated with the diffusion and charge transfer effects and (ii) not stationary while under operation, that is, when the battery cell is actively charged or discharged. If EIS is used for making an online diagnosis (i.e., when the battery is working in its application environment), very restricted experimental conditions must be adopted to adequately approximate the requirements stated above.

Linearity is fulfilled when the amplitude and the phase response of the system under test do not depend on the magnitude of the excitation signal. For battery cells, this means that a small excitation amplitude should be used so that the behavior of the system can be assumed to be linear in a certain operating region with an acceptable inaccuracy level. Given the very low level of resistance provided by a typical battery cell, the implementation of a current excitation is easier and more accurate than a voltage one; therefore, the battery is usually excited with a current in the mA to A range [15] but it should be as small as possible to assume that the battery is working in the linear regime [23]. Although the linearity constraint is generally considered easier to enforce in the single sine case, in the multisine scenario, it is sufficient to ensure that the overall multisine signal remains within acceptable bounds by monitoring its peak value.

Stationarity is achieved when all transients fade out and the "steady-state" condition is reached. Conventional EIS performed at the laboratory-level complies with this time-consuming condition, while during battery operation in online applications, the quasi-stationarity approximation has to be considered, which implies shortening the measurement time to assume that the internal state of the cell does not change significantly during the measurement process. As for multisine excitation, all frequencies are applied simultaneously within a relatively fast period of time, so the quasi-stationarity hypothesis is respected.

The conformity of an impedance spectrum to the constraints of linearity and stationarity is typically checked through the Kramers–Kronig relations [24], which relate the real and the imaginary component of the impedance value. The direct application of such relations requires integration over the frequency range from zero to infinity, but practical EIS measurements involve a finite frequency range, thus approximations usually rely on measurement models employed to check the compatibility of the impedance data with the Kramers–Kronig relations. Kramers–Kronig analysis is a valuable tool to validate the sine sweep impedance data; while it was first suggested in [25] and then empirically shown in [26] through measurements and numerical simulations, multisine impedance data always satisfy the Kramers–Kronig conditions, so they cannot be used as a verification method. To inspect nonlinearity and non-stationarity in multisine impedance spectra, a full Fourier domain analysis is necessary. For example, the inherently nonlinear and non-stationary behavior of electrochemical systems is easily detected by applying an odd random phase multisine excitation and studying the measured frequency domain data [27].

Alternative solutions have been developed during the last decade to estimate nonlinear and time-varying impedances, which make use of advanced algorithms [28,29] but are not covered in this work. A random phase multisine excitation was implemented in this study, together with a dedicated discrete Fourier transform (DFT) algorithm.

2.2. Crest Factor

By definition, a multisine signal is expressed as the sum of purely sinusoidal contributions as follows:

$$x(t) = \sum_{i=0}^{N_T-1} A_i \cos(2\pi f_i t + \phi_i). \quad (1)$$

The available degrees of freedom when designing the excitation signal include the amplitudes A_i, frequency f_i, and phase ϕ_i of each individual component, along with the total number N_T of frequency components.

Given this definition and the number of parameters involved, the multisine signal can be properly designed to concentrate the excitation power into selected frequency components and achieve specified SNR values for each frequency [20].

In impedance spectroscopy, the excitation signal must remain within the linearity region of the device under test, which generally limits its maximum amplitude. Conversely, the individual tone amplitudes A_i should be maximized to achieve sufficient SNR and ensure adequate accuracy. Therefore, after the determination of the number of frequency components N_T and amplitudes of the tones A_i, the phases ϕ_i should be properly designed to minimize the peak value of the overall multisine signal, that is, $X_{peak} = max\{|x(t)|\}$. The variable used to describe the relationship between the phases and peak value of the multisine is the crest factor (CF), defined as the ratio of the peak value to the signal root mean square (RMS) value X_{RMS}. For a signal $x(t)$ measured over a time interval [0,T], the CF is estimated according to the following formula:

$$CF = \frac{X_{peak}}{X_{RMS}} = \frac{\max(|x(t)|)}{\sqrt{\frac{1}{T}\int_0^T x(t)^2 dt}} \quad (2)$$

For a single sine wave, the crest factor is $\sqrt{2}$, and the phase does not play any role. As a common practice and for ease of implementation, the amplitudes A_i of the individual components of the multisine signal defined in (1) are kept at the same value A, then the RMS values $X_{RMS,i}$ of all the components are equal to each other, and the RMS value of the sum of the sine waves depends only on the value A and the number N_T of components:

$$X_{RMS} = \sqrt{\sum_{i=0}^{N_T-1} X_{RMS,i}^2} = \sqrt{\sum_{i=0}^{N_T-1} \frac{A_i^2}{2}} = \frac{A\sqrt{N_T}}{\sqrt{2}} \equiv X_{RMS,i}\sqrt{N_T}. \quad (3)$$

However, the peak value X_{peak} of the multisine signal also depends on the phases ϕ_i of the frequency components. Thus, the CF optimization is crucial to finding the optimal set of phase values, which ensures the minimum peak value X_{peak} of the multisine signal at the same RMS value X_{RMS}. Alternatively, the RMS value of each i-th frequency component can be related to the signal amplitude as:

$$X_{RMS,i} = \frac{X_{peak}}{\sqrt{N_T} CF}. \quad (4)$$

The lower the CF, the higher the energy throughout the measurement time per tone for a given multisine peak value. A high energy per tone means that the signal is less susceptible to noise, thus improving the impedance measurement quality. In most cases,

an optimization procedure of the crest factor is necessary to ensure a good SNR. State-of-the-art methods for reducing *CF* can be divided into three main categories: direct or analytical methods, iterative methods, and meta-heuristic methods. Analytical methods can typically return the phases directly. One of the first analytical strategies was proposed by Schroeder [30]. The Schroeder algorithm uses a single-shot, closed formula by choosing the initial phase values of a flat-power spectrum signal, resulting in an acceptable *CF* for signals with a uniform distribution of frequency components. For a multisine signal with non-uniform distribution, the strategy does not produce better results than simply choosing random initial phase values. The Littlewood and Newman formulae also apply to multisine signals with equidistant amplitude spectrum and are unsuitable for multisine signals with arbitrary or logarithmically distributed frequencies [31]. Iterative methods are more computationally expensive but can achieve better *CF* values. Van der Ouderaa (VDO) [31] and Yang [32] described a fast Fourier transform (FFT)-based method where a continuous exchange between the time- and frequency-domain was applied with nonlinear time-domain clipping and frequency-domain filtering. Guillaume [33] proposed another method where Lp norms of the time-domain multisine signal are used as an optimization objective for the Gauss–Newton algorithm. Various attempts have been made to improve the results of the Schroeder and VDO algorithms by also utilizing combinations of the analytical formula and/or numerical iteration methods [20,34,35]. However, the optimization was carried out for a relatively low number of sinusoidal components. Currently, no iterative optimization algorithm is capable of returning signal optimization with a reasonable number of iterations. Meta-heuristic methods are based on evolutionary principles, starting with a population of randomly generated initial phases that are progressively optimized over successive generations. Techniques such as the genetic algorithm [36] and artificial bee colony [37] have been applied to optimize the crest factor. These meta-heuristic approaches typically yield solutions close to the global optimum and often perform as well as or better than deterministic methods. However, their main drawback is the significant time required, as they can take several days to run when applied to Li-ion battery excitation signals. Recently, hybrid stochastic-deterministic optimization algorithms have also been introduced [38].

The solution to the *CF* problem, which consists of selecting the optimal set of starting phases of the frequency components, remains a challenge to this day. However, even if *CF* minimization is crucial for the optimal measurement setup, the choice of the optimization method does not affect the excitation strategy proposed in this study.

3. Multiband Multisine Excitation Strategy

Although the multisine is one of the most energy-efficient signals and *CF* optimization algorithms allow for the maximization of the energy on a single tone, the limitation on the amplitude set by the linearity hypothesis may affect the measurement accuracy. Moreover, an EIS system with limited hardware resources could set a further limitation on the peak value of the excitation signal or could introduce quantization-related errors that also affect the measurement accuracy. To overcome this problem, it is possible to divide the bandwidth of interest into K sub-bands, each one investigated sequentially by using different multisine signals that excite a subset of $N = N_T/K$ frequency tones. A graphic representation of the proposed multiband multisine concept is shown in Figure 1c. With this method, it is possible to concentrate, during each measurement step, the maximum energy available from the excitation source onto a smaller number of tones (in analogy with the sine sweep technique, Figure 1a), thus improving the SNR and accuracy in the estimation of each frequency point of the impedance spectrum while preserving a still acceptably short overall measurement time with respect to that potentially offered by a

single-band multisine technique (Figure 1b). In other words, the proposed multiband multisine excitation technique represents the optimal trade-off between the accuracy and measurement time, which makes the implementation of online EIS investigation at the battery cell-level feasible.

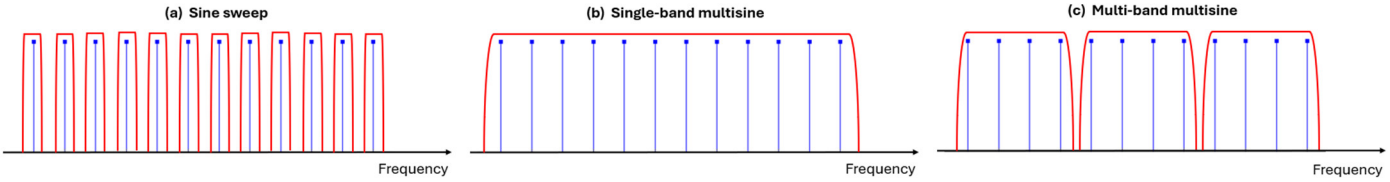

Figure 1. Multiband multisine excitation method compared with the classical sine sweep and single-band multisine. The red contours identify each excitation step in the EIS investigation.

3.1. Measurement Time

In the sine sweep technique, the measurement time needed to excite the entire frequency bandwidth, not including delays of other nature (e.g., computation times), is usually defined as $\overline{T}_{meas,sweep} = N_P \sum_{i=0}^{N_T-1} 1/f_i = N_P \sum_{i=0}^{N_T-1} T_i$, where N_P is an integer of the number of periods the signal must complete for proper excitation. However, from a practical standpoint, any architecture used to generate the excitation signal takes a short time-lapse to change the frequency parameter to the next one. This waiting time, T_w, can be negligible or not, depending on the specific system implementation. However, it should be considered in the calculation of the total measurement time, as follows:

$$T_{meas,\,sweep} = N_P \sum_{i=0}^{N_T-1} T_i + (N_T - 1)T_w \tag{5}$$

For broadband signals such as the multisine signal, the lowest frequency is the one that most affects the excitation time, thus the measurement time can be approximated to N_P periods of the sinusoidal component at the lowest frequency f_{min}:

$$T_{meas,\,single-band} = N_P(1/f_{min}) = N_P T_{max} \tag{6}$$

Following the same criteria, in the proposed multiband multisine excitation technique, the measurement time of the j-th sub-band can be approximated as the excitation time $N_P T_{max,j}$ of the component at the lowest frequency of the sub-band. Then, the total measurement time can be estimated by summing the excitation times of each sub-band and adding the time needed to switch between sub-bands. Assuming that such a time-lapse originates from the system implementation as before, we named it T_w again. It is reasonable to expect that the hardware resources can manage the switching time between the sub-bands with sufficient speed to be considered practically negligible, particularly compared with the sub-band with a lower frequency. This assumption is fundamental to preserve the validity of the method as it ensures that the transition between bands does not introduce significant delays that could affect the measurement in the online approach. In this study, the same number of frequency points, or tones, N in each sub-band of the multiband multisine was considered, so the total measurement time can be expressed as:

$$T_{meas,multi-band} = N_P \sum_{j=0}^{K-1} T_{max,j} + (K-1)T_w \tag{7}$$

In Table 1, the total measurement time of the proposed technique was compared with those of the conventional sine sweep and single-band multisine by also making explicit the most burdensome time contribution $N_P T_{max,0} \equiv N_P T_{max}$.

Table 1. Comparison of the excitation techniques in terms of the measurement time and RMS value of a single tone.

Excitation Technique	Measurement Time	Single Tone RMS
Sine sweep	$T_{meas,sweep} = N_P T_{max} + N_P \sum_{i=1}^{N_T-1} T_i + (N_T - 1)\, T_w$	$X_{RMS,i} = \frac{X_{peak}}{\sqrt{2}}$
Single-band multisine	$T_{meas,single-band} = N_P T_{max}$	$X_{RMS,i} = \frac{X_{peak}}{\sqrt{N_T}\, CF}$, $CF > \sqrt{2}$
Multiband multisine	$T_{meas,multi-band} = N_P T_{max} + \sum_{j=1}^{K-1} T_{max,j} + (K-1) T_w$	$X_{RMS,i} = \frac{X_{peak}}{\sqrt{N}\, CF}$, $CF > \sqrt{2}$

3.2. Energy-Efficiency

The comparison in terms of SNR between the three techniques was carried out by assuming the same limitations in terms of the maximum allowed peak value of the excitation signal and noise level. Under these hypotheses, the SNR of each single frequency component can be directly related to the RMS value of the same frequency tone. In other words, maximization of the SNR turned out to be a problem of maximizing the energy on each frequency tone.

For the sine sweep method, the RMS value of a single tone is easily derived as $X_{RMS,i} = X_{peak}/\sqrt{2}$. The single-band multisine case has already been dealt with in Section 2, where Equation (4) defines how to obtain the RMS value for each tone, considering that the *CF* always assumes values higher than $\sqrt{2}$. A similar equation can be derived for the multiband multisine method by simply substituting the total number of components N_T with the effective number of tones N contained in a single sub-band:

$$X_{RMS,i} = \frac{X_{peak}}{\sqrt{N} CF}\,. \tag{8}$$

All the cases are summarized in the second column of Table 1. From the table, and assuming that the same minimum *CF* value can be obtained by the same source for both the multisine and multiband cases, it is clear to infer that the proposed multiband multisine technique is an intermediate solution that tries to obtain the best trade-off between measurement time and accuracy.

4. Design of Multiband Multisine Sequence

According to the analysis given above, the proposed method is not the optimum solution in terms of measurement time nor energy efficiency, but it allows for a trade-off between the measurement time and single-tone RMS value to be obtained in relation to specific requirements and limitations set by the hardware technology or the application. This section shows how to exploit the multiband multisine strategy starting from defined constraints. More precisely, it examines the case in which the maximum value for the peak of the excitation signal and the overall noise level are set by the EIS-based sensing system and the specific battery cell under test. The first step of the process involves the choice of the frequency points in the bandwidth of interest for the impedance monitoring and their spacing. Then, an optimization procedure of the *CF* of the signal follows, considering a set of possible values for the minimum RMS required for each frequency tone.

4.1. Frequency Components and Spacing

To maximize the extracted information about the frequency domain behavior of the battery for online diagnosis, special care must be taken in the choice of the frequency points to be excited. To preliminarily validate the proposed approach by means of simulations, the study focused on the band B = [1–10] Hz by considering it as one of the sub-bands of the overall multiband multisine signal. Using logarithmic spacing in this frequency band results in uneven or impractical frequency points for the tones to be evenly distributed. In contrast, linear spacing is more advantageous, as it ensures a perfectly even distribution of tones while using simple and convenient frequency values.

Moreover, from the *CF* optimization perspective, it was noticeable that the linear frequency spacing can be optimized to significantly lower *CF* values compared with signals with (quasi-)logarithmic spacing [19,39]. In the simulation, N assumes the values (1, 2, 4, 5, 10), while the excitation signal is sampled at frequency F_S fixed to 200 kHz, much higher than the excitation band. Each excitation signal is thus represented by L samples, where L varies with the number of sinusoidal tones in the excitation signal to ensure coherent sampling. In Table 2, the design parameters related to the frequency components are summarized for each multisine excitation signal.

Table 2. Design parameters in the sub-band B = [1–10] Hz for the set of multisine signals used in the simulation.

No. of Tones (*N*)	Frequencies (Hz)	Fs (kHz)	No. of Samples (*L*)
1	[5]	200	40,000
2	[3, 9]	200	66,666
4	[2, 4, 6, 8]	200	100,000
5	[1, 3, 5, 7, 9]	200	200,000
10	[1, 2, 3, 4, 5, 6, 7, 8, 9, 10]	200	200,000

4.2. Amplitude and CF Optimization

The minimization algorithm of the *CF* of the multisine signal was implemented in MATLAB® R2024A by using the fdident toolbox and following the VDO method [31]. This algorithm iterates toward an optimum set of phases for which the *CF* of the multisine with the given amplitudes is the minimum. This method is based on swapping between the time and frequency domain: the time domain waveform is clipped, then transformed to the frequency domain, and the amplitude is restored to the desired values. The clipping level (which is defined as a percentage of $max(|x(t)|)$, typically between 75% and 95%) is slightly adjusted according to the evolution of the *CF* (i.e., when the result is improved, the clipping level is decreased, otherwise it is increased). The algorithm was set to perform 10^4 iterations starting from a set of random phases. The number of tones N and the frequencies f_i of the multisine signals were set following Table 2, together with the parameters F_S and L. The amplitudes of the frequency components were kept at the same level in the process, assuming that the additive noise was white throughout sub-band B (i.e., for achieving the minimum, equal SNR on each tone that is required by the application it suffices to impose the same $X_{RMS,i}$). Four normalized values $X_{RMS,i}$ = [1, 2, 4, 8] were used in the following example. The used toolbox allowed us to arbitrarily choose the $X_{RMS,i}$ value, automatically scaling the generated signal. In Figure 2, the results for N = 4 tones and $X_{RMS,i} = 4$ $(i = 0, 1, 2, 3)$ are shown in both the time domain and frequency domain. Specifically, the obtained values of the *CF* and the X_{peak} of the signal confirm the relation expressed in Equation (8).

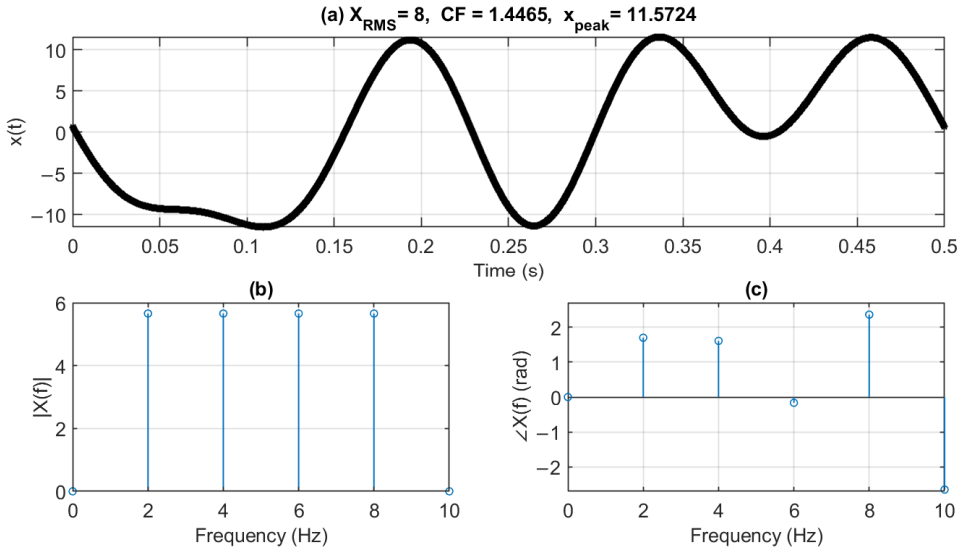

Figure 2. Amplitude and *CF* optimization algorithm applied to the multisine signal in sub-band B = [1–10] Hz when N = 4 and $X_{RMS,i} = 4$. The signal is shown in the time domain (**a**) and in the frequency domain by magnitude (**b**) and phase (**c**).

4.3. Simulation Results

The overall results of the *CF* optimization algorithm for the simulated set of N and single-tone RMS are reported in Figure 3. They can be read in two different ways, depending on the scenario the user must face. In the first, shown in Figure 3a, the aim is to find the required value of the (current) excitation signal $X_{peak} = I_{max}$ according to the chosen number of tones N for each sub-band of the multisine sequence and to the desired $X_{RMS,i}$. In the second, represented in Figure 3b, the operative parameter to be extracted is the maximum number of tones N_{max} that one can excite in a sub-band when the amplitude of the excitation signal is limited to I_{max} and a specific minimum $X_{RMS,i}$ value (i.e., a SNR, i level) is requested. Both the excitation current I_{max} and the RMS values are expressed in arbitrary units, since the goal of this discussion is to present the working principle of the multiband strategy; units can be then customized to the requirements and specifications of the available HW/SW EIS system.

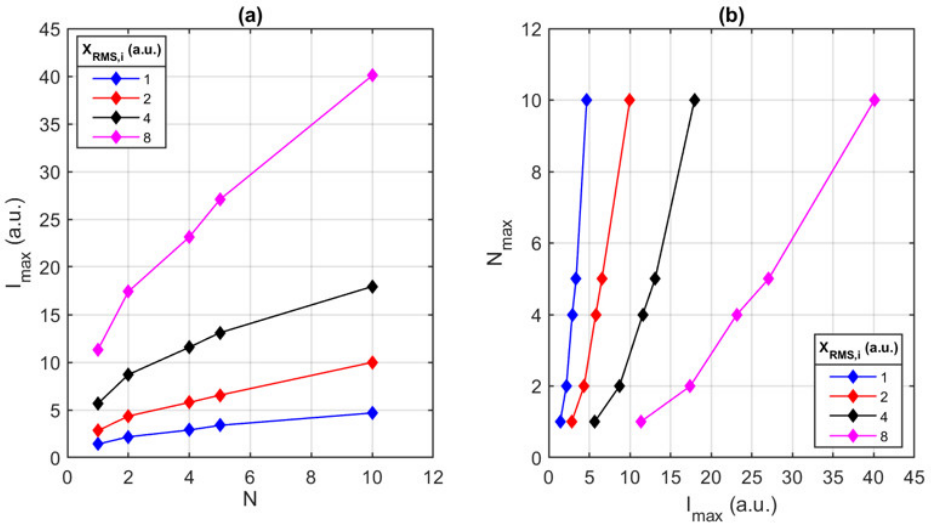

Figure 3. (**a**) Maximum current excitation value in relation to the number of tones and the desired single-tone RMS value. (**b**) Maximum number of tones in the sub-band in function of the maximum current excitation available/exploitable for linearity purposes and the desired single-tone RMS value.

5. Numerical Tests and Experimental Examples

5.1. Co-Simulation Framework

To test the proposed excitation strategy, the architecture presented in [18,40] was refined in terms of hardware and SW-implemented in the co-simulation framework presented in [41]. The latter is an integrated numerical framework that combines a CAD circuit simulator of the hardware architecture of an EIS-based sensing system (including the model of the battery cell under test) and an environment for the post-processing of data provided by the hardware analyses to obtain the final estimate of the cell impedance spectrum. Such a numerical framework can simulate a complete EIS system with an arbitrary excitation pattern, simply uploading the excitation signal designed as input to the DAC used for the generation of the test signals. Moreover, it takes into account not only the non-idealities and sources of uncertainty in both the hardware (HW) and software (SW) sub-sections, but also those that are generated due to the inherent interrelations between them. Thus, it consists of an actual digital twin of the overall sensing system, being an excellent and flexible environment to compare, in particular, different excitation techniques and validate them as efficient excitation methods to perform online EIS.

Figure 4 shows the general structure of the co-simulation framework. The circuit simulator of the HW architecture has four inputs: the description of the analog circuit, the description of the analog-to-digital converters (ADCs), the battery model, and the excitation pattern. The specific architecture implemented for the present work consisted of a 1-bit Delta-Sigma current digital-to-analog converter (DAC), a bandpass filter, and two identical measurement channels: one used to sense the voltage drop across the battery cell and the other used to sense the voltage across a reference resistor. The acquisition chain included instrumentation amplifiers and high-resolution digitizers, which were modeled as ideal ADCs in Verilog-A. A commercial battery cell was modeled with a fractional-order ECM whose parameters were experimentally extracted by means of measurements carried out with the Hioki IM3590 Chemical Impedance Analyzer connected to a fully-charged cylindrical lithium-ion battery cell Samsung ICR18650-26J 2600 mAh (Figure 5). The main input to the numerical environment was the algorithm used to estimate the impedance spectrum based on the raw data provided by the HW simulator. Such a custom algorithm, already presented in [18], was based on the FFT and on a peak search algorithm to identify the harmonic components of interest.

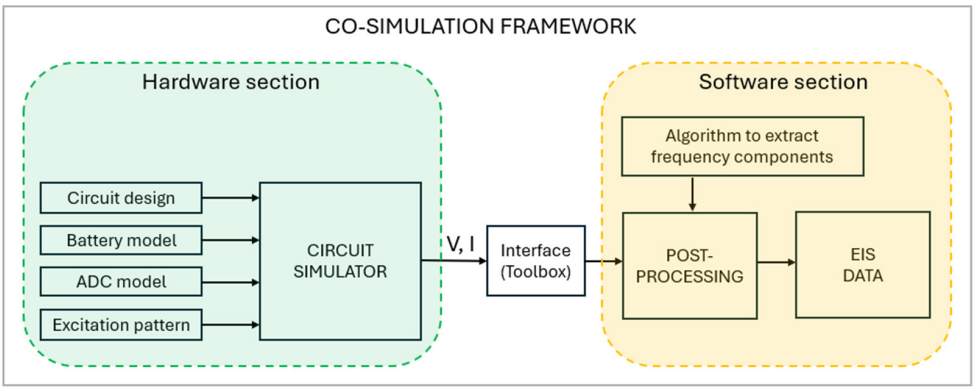

Figure 4. Block scheme of the co-simulation framework presented in [41] and used in this work.

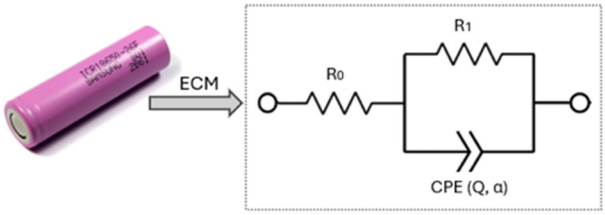

Figure 5. Equivalent circuit model of the fully-charged battery cell Samsung ICR18650-26J used in the simulation framework. Values of the parameters were experimentally extracted using a Hioki IM3590 Chemical Impedance Analyzer.

5.2. Multiband Multisine Excitation Signal Design

For lithium-ion batteries, the most interesting frequency region of the impedance spectrum is from 0.01 Hz to 1000 Hz [3,21], where electrochemical and physical processes mainly occur. This is the typical bandwidth explored in EIS-based tests performed at the laboratory-level, with the cell in quiescent conditions after a suitably long relaxation time. However, for online battery cell diagnosis, when the cell is working under the operating conditions forced by the application, the investigated region must be reduced to shorten the measurement time in order to guarantee the time-invariancy conditions of the cell state during the observation while preserving adequate spectral information, by focusing on the most informative portion of the impedance spectrum. A lower excitation frequency of 1 Hz is commonly chosen in the online EIS of battery cells [10,42,43], while a higher frequency point is usually limited by the hardware implementation [18]. In the following, the selected bandwidth for the simulation tests covered the range [1–100] Hz. Higher sub-bands could be easily introduced, but the time needed to apply them be-comes practically negligible when compared with that associated with the range [1–100] Hz, since it would only introduce additional waiting times T_w, which were dealt with as purely HW-dependent parameters in this work (see Section 3.1 and Table 6 in the following).

Firstly, the single-band multisine signal was designed by choosing an arbitrary number of tones $N_T = 20$ in the frequency bandwidth. Following the same approach as the previous simulations, the frequency points were linearly spaced. Even if logarithmic frequency spacing is commonly chosen in battery cell diagnosis to monitor the different phenomena in the impedance spectrum, logarithmically spaced signals show an inherently higher *CF* and therefore are not the best choice to demonstrate the validity of the proposed study. Moreover, the selected bandwidth was still small enough to allow for a good investigation with linear spacing. The *CF* minimization procedure was performed by setting the RMS value of the single tone $X_{RMS,i}$, so the single-band multisine signal was $X_{RMS} = 4.47$ and had a peak of 7.97 a.u. The result of the minimization algorithm, together with the parameters of the single-band multisine sequence, is summarized in Table 3. The signal in the time- and frequency-domains is depicted in Figure 6. Since the lowest frequency was 1 Hz, the minimum measurement time was 1 s for the single-band multisine when $N_P = 1$.

Table 3. Parameters of the single-band multisine sequence designed for the simulation with the numerical framework.

Frequencies (Hz)	Fs (kHz)	Nr. of Samples (*L*)	X_{RMS} (a.u.)	CF	X_{peak}(a.u.)
[1, 6, 11, 17, 22, 27, 32, 37, 43, 48, 53, 58, 64, 69, 74, 79, 84, 90, 95, 100]	200	200,000	4.47	1.7831	7.9703

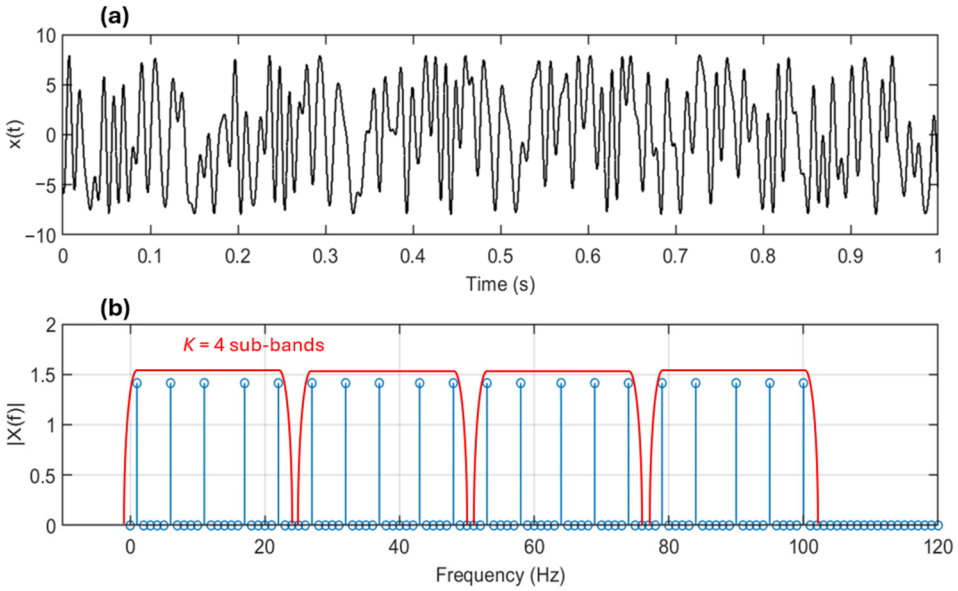

Figure 6. Amplitude and *CF* optimization algorithm applied to the multisine signal in bandwidth B = [1–100] Hz when N_T = 20 and $X_{RMS,i} = 1$. The signal is shown in the time domain (**a**) and in frequency domain (**b**). A multiband technique was implemented by dividing the frequency band in K = 4 sub-bands as shown in (**b**).

To implement the multiband technique, the same frequency band of interest was divided into sub-bands of N = 5 tones each, resulting in K = 4 sub-bands (Figure 6b). The number of tones and their frequency location were chosen in accordance with the single-band case described above. An arbitrary choice is possible in this simulation, where the amplitude of the excitation signal is fixed and limited by the EIS-based circuit implemented in the framework, and the RMS value of the excitation signal is user-selectable in the *CF* minimization procedure. In a real application, the optimal number of tones N derives from an accurate evaluation of the available excitation current I_{max} and the desired RMS value, as presented in the simulation results in Section 4.3 (see Figure 3). The design of each sub-band multisine signal was obtained with the same algorithm implemented for the single-band multisine. For a proper comparison between the two techniques, the X_{peak} value of each sub-band multisine signal was fixed to the same value as the single-band multisine signal (i.e., $X_{peak} = 7.9703$a.u.), thus the RMS values $X_{RMS,i}$ were derived from Equation (8). The details of each sub-band sequence are shown in Table 4.

Table 4. Sub-band multisine sequences designed for the simulation with the numerical framework.

j-th Sub-Band	Frequencies (Hz)	$X_{RMS,i}$ (a.u.)	*CF*	X_{peak}(a.u.)
j = 0	[1, 6, 11, 17, 22]	1.79	1. 8971	7.9703
j = 1	[27, 32, 37, 43, 48]	1.88	1.6926	7.9703
j = 2	[53, 58, 64, 69, 74]	1.87	1.9179	7.9703
j = 3	[79, 84, 90, 95, 100]	1.98	1.9976	7.9703

5.3. Impedance Estimation

The comparison between the two excitation techniques was carried out by looking at the impedance values estimated by the framework described in Section 5.1. In Figure 7, the impedance spectrum of the battery cell is represented both in the Cole–Cole plot (Figure 7a) and in the Bode diagrams (Figure 7b,c). The results of the single-band multisine excitation (cyan circles) and the multiband excitation (blue squares) were compared with the

reference analytically provided by the battery ECM (red points) over the frequency points of interest. The proposed multiband multisine method clearly demonstrated better accuracy in the impedance estimation with respect to the classical method, as the frequency points estimated by the multiband multisine signal fit the reference curve better. In Figure 8, the estimation errors of the magnitude and phase of the battery impedance over the frequency range are reported for both techniques computed as the difference with respect to the battery ECM. The RMSE of the impedance magnitude improved from 7.30 mΩ for the single-band multisine to 0.40 mΩ for the multiband multisine approach, while the RMSE of the impedance phase improved from 67.8 mrad to 4.9 mrad. This simulation example, which takes into account the overall HW + SW components of the EIS-based sensing system, demonstrates that, with equal parameters of I_{max} and noise level, the use of the multiband multisine excitation leads to a better estimation of the battery spectrum on the very same frequency tones.

Furthermore, to emphasize the importance of performing the *CF* optimization procedure for each sub-band of the multiband multisine signal, the impedance estimates obtained using the proposed multiband excitation were compared with those derived from a sub-band design that had not been optimized with the *CF* algorithm (magenta diamonds in Figure 7). In this case, the sub-band multisine signals, generated using the *idinput* MATLAB® function, were designed by selecting random phases that provided the smallest signal amplitude and frequencies equally spread over a custom frequency grid. With an RMSE of 0.47 mΩ and 11.2 mrad for the magnitude and for the phase, respectively, this method was confirmed to be less accurate than the *CF* optimized sub-band design. All of these results are summarized in Table 5 for synoptical comparison.

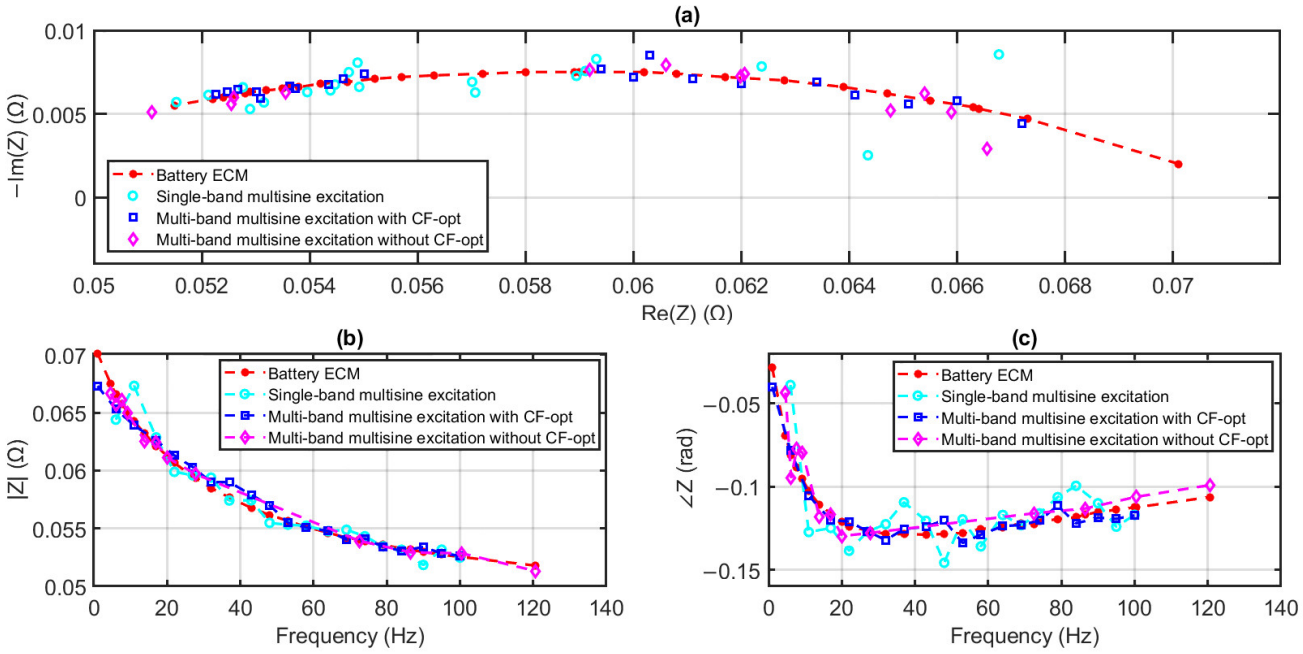

Figure 7. Impedance data of the battery cell estimated by the co-simulation framework are shown in the Cole–Cole plot (**a**) and in the Bode diagrams in magnitude (**b**) and phase (**c**). The single-band multisine excitation method was compared with the multiband multisine excitation method considering the sub-band design with both the *CF* optimization procedure and without the *CF* optimization. The battery ECM impedance spectrum is shown as a reference.

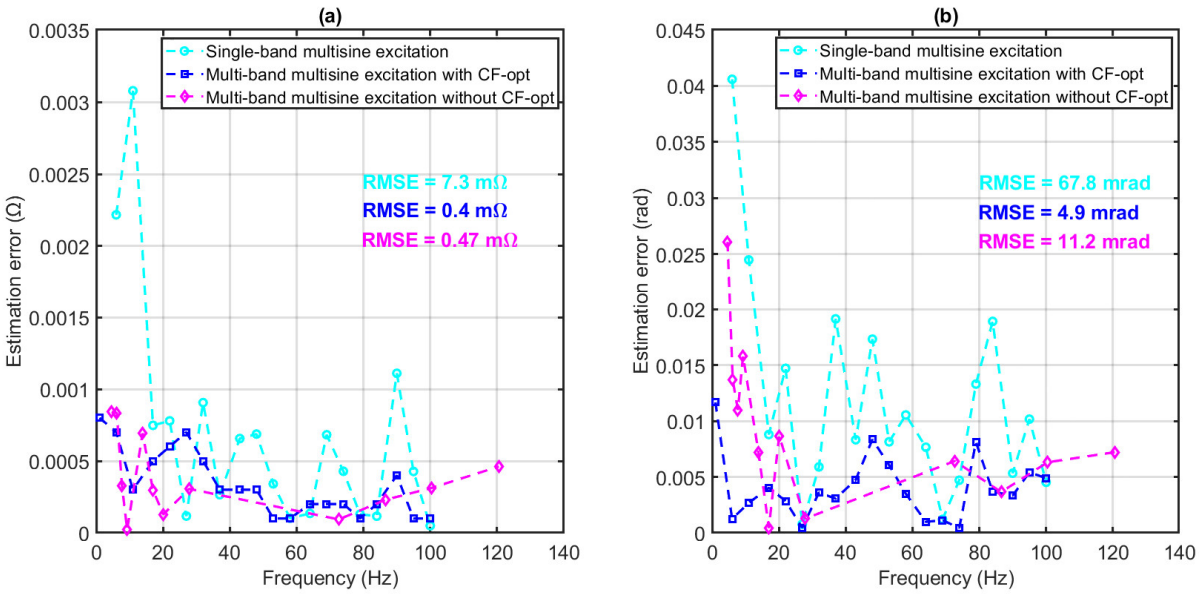

Figure 8. Errors of the estimated values of magnitude (**a**) and phase (**b**) of the battery impedance when comparing the simulation results and battery ECM.

Table 5. RMS errors of the estimated impedance values in magnitude and phase when comparing the simulation results for the classical (single-band) and proposed (multiband) excitation techniques with the battery ECM analytical spectrum.

Excitation Technique	Magnitude RMSE (mΩ)	Phase RMSE (mrad)
Single-band multisine	7.30	67.8
Multiband multisine with *CF* optimization	0.40	4.9
Multiband multisine without *CF* optimization	0.47	11.2

Further considerations must be made regarding the measurement time needed to investigate the frequency bandwidth considered when comparing the two excitation techniques and also including the sine sweep method described in Section 3.1. An arbitrary number of periods of the signal $N_P = 10$ was considered, while the waiting time T_w, which depends on the system implementation was left as a parameter. To excite the same frequency points in Tables 3 and 4, the sine sweep technique took $16.4 + 19\ T_w$ seconds while the multisine technique took only 10 s. The multiband multisine technique took a little more than 10 seconds, but was faster than the sine sweep. The calculated measurement times are shown in Table 6.

Table 6. Comparison between the excitation techniques in terms of measurement time needed to investigate the frequency bandwidth considered.

Excitation Technique	Measurement Time (s)
Sine sweep	$T = N_P \sum_{i=0}^{N_T-1} T_i + (N_T - 1)\ T_w = N_P\ 1.64 + 19\ T_w = 16.4 + 19\ T_w$
Single-band multisine	$T = N_P\ T_{max} = N_P\ 1 = 10$
Multiband multisine	$T = N_P \sum_{j=0}^{K-1} T_{max,j} + (K-1) T_w = N_P\ 1.07 + 3\ T_w = 10.7 + 3\ T_w$

Table 6 shows how the proposed technique allowed for a still short measurement time to be preserved when compared with the fastest single-band method while offering better accuracy (see Table 5), thanks to the higher SNR values obtained at the frequency points investigated.

To demonstrate the practical feasibility of the proposed multiband multisine excitation method, it was implemented using the hardware prototype described in [18] and experimentally assessed in the framework of an automotive-grade laboratory environment. Specifically, a commercial cylindrical 18650 lithium-ion cell with 3.6 V nominal voltage, 2.9 Ah nominal capacity, and 2.5–4.2 V voltage limits was monitored during the capacity check test, which is part of a standard industrial procedure known as the Reference Performance Test (RPT) [44], and performed to quantitatively assess the SoH of the cell after a given aging cycle by measuring key parameters such as capacity, internal resistance, and discharge efficiency [45] under controlled conditions (e.g., at constant ambient temperature). In this case, the capacity check involved a CCCV charge at a C-rate 1/3 up to 4.2 V and a CC discharge at a C-rate 1/3 down to 2.5 V. The online EIS measurement using the prototype with multiband multisine excitation was performed at different values of battery voltage during the charge and discharge cycles of this capacity check. The investigated frequency band was [4–100] Hz and the frequencies were arranged in K = 3 sub-bands of N = 4 tones each: $B_{(j=0)}$ = [4, 6, 7, 9] Hz, $B_{(j=1)}$ = [14, 16, 20, 27] Hz, $B_{(j=2)}$ = [70, 80, 90, 100] Hz. In Figure 9, the estimated impedance is shown during the discharging (Figure 9a) and charging (Figure 9a). Both the trends of the battery impedance were correctly identified by the measurement system, proving the capability of the proposed excitation technique to monitor the battery cell state time-evolution online during operation.

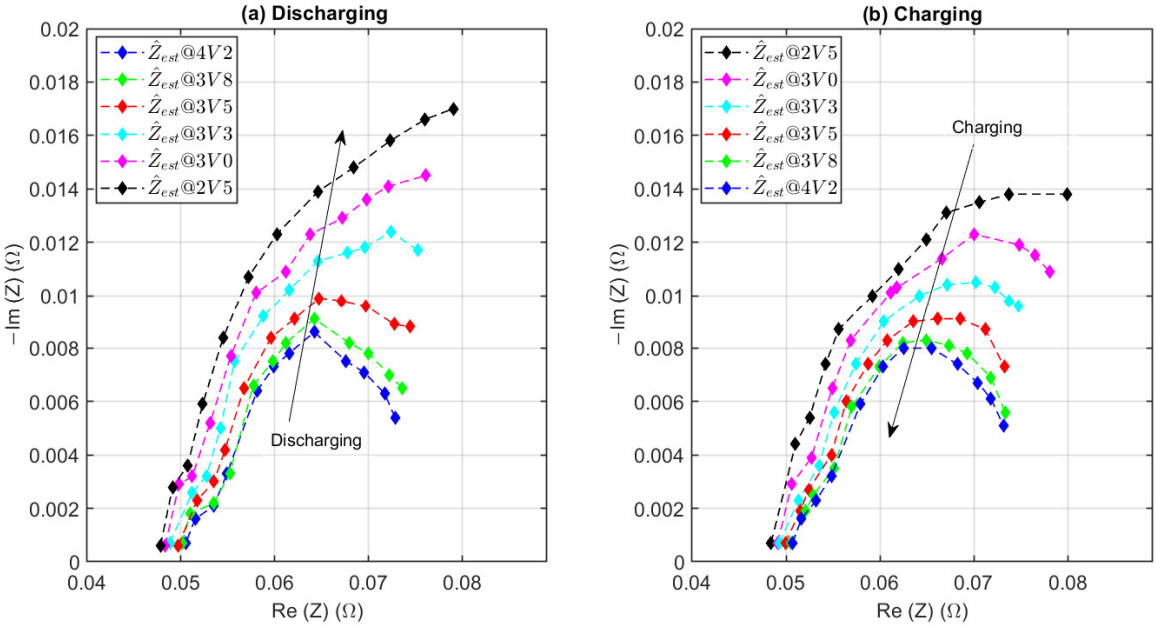

Figure 9. Experimental online acquisition of the impedance spectrum by the EIS sensing system presented in [18] and implementation of the multiband multisine excitation method during the capacity check discharge (**a**) and charge process (**b**) of a commercial cylindrical 18650 lithium-ion cell.

6. Conclusions

In this paper, a novel technique to perform broadband online EIS on battery cells based on a multiband multisine excitation signal was presented. The innovative approach consists of dividing the overall spectrum of interest into sub-bands to be sequentially excited with different multisine signals, thus concentrating, at each step, the energy of the perturbation

source in a smaller number of frequency tones with respect to a single-band multisine technique. The multiband technique resulted in being faster than the conventional sine sweep and just slightly slower than the single-band multisine excitation, thus being a reliable method for the real-time diagnosis of the battery state. In terms of energy efficiency, the sub-band division allowed for a higher SNR for a single frequency component to be obtained with respect to the single-band multisine signal. Even if it does not reach the efficiency of the sine sweep, by properly choosing the number of frequency points and following an optimization procedure of the CF, the impedance measurement accuracy can be considerably improved. The choice of the maximum number of tones N_{max} excited in each sub-band is related to the available amplitude of the excitation signal I_{max} and the required RMS for single-frequency tone $X_{RMS,i}$. In the first part of this work, the implemented simulation showed how it is possible to find the best combination of these three parameters when limitations due to the hardware technology or the application must be faced.

Preliminary tests with the proposed strategy were carried out by means of a numerical simulation framework used as an EIS-based measurement system for battery cell monitoring, where a commercial cell was modeled with a fractional-order ECM. The battery impedance spectrum was estimated by both the single-band multisine excitation and the proposed technique and investigated the same frequency range (i.e., [1–100] Hz) and exciting the same frequency points. With equal parameters of I_{max} and RMS of the excitation signal, the RMSE of the estimated impedance with respect to the ECM assumed lower values when implementing the multiband approach. Additionally, the accuracy of the impedance measurement was higher when the sub-band multisine signals were designed following the *CF* minimization algorithm. Moreover, a new practical design method regarding the frequency distribution of the excitation signal can be deduced from this study. Since the interesting spectrum of the battery can extend to the [0.1 Hz–1000 Hz] range, with multiband excitation, it is possible to select sub-bands logarithmically spaced to each other to cover the entire spectrum and at the same time choose a linear frequency distribution for each sub-band to optimize the CF. These results, together with the comparison of the effective measurement times calculated for each excitation technique, confirm that the proposed multiband multisine strategy is a trade-off solution in terms of the measurement time and accuracy with respect to the single-band multisine and the sine sweep excitations. It represents a promising choice for the real-time monitoring of the electrochemical impedance of battery cells with adequate accuracy and in reduced times, compatible with online applications.

From an implementation point of view, the proposed strategy does not introduce any further limitations. Assuming that the excitation sequences are pre-calculated offline, the level of complexity in the realization of the overall excitation is not a problem, while the amount of required memory is increased by a factor K, but is not an issue given the capabilities of state-of-the-art microcontroller-based digital systems. The sequential application of the sub-bands in place of a single-band is not an issue for both present and future hardware. The challenges are those typical of integrated sensing, specifically the EIS sensing integration on the BMS, which is an active research topic for next-generation BMSs [14,46,47]. The work presented in this paper could be applied to improve such activities.

As a result, the proposed methodology constitutes a robust solution for real-time, embedded, and *in situ* battery diagnostics, with significant implications for the design of BMSs, the implementation of predictive maintenance frameworks, and the reinforcement of safety protocols in energy storage technologies.

Author Contributions: Conceptualization, R.R., M.C. and P.A.T.; methodology, R.R., M.C. and P.A.T.; software, R.R. and N.L.; validation, R.R. and N.L.; formal analysis, R.R., M.C. and P.A.T.; investigation, R.R., M.C. and P.A.T.; resources, R.R. and N.L.; data curation, R.R. and N.L.; writing—original draft preparation, R.R., M.C. and P.A.T.; writing—review and editing, R.R., M.C. and P.A.T.; visualization, R.R.; supervision, M.C. and P.A.T.; project administration, M.C. and P.A.T.; funding acquisition, M.C. and P.A.T. All authors have read and agreed to the published version of the manuscript.

Funding: This work was co-funded by the Italian Ministry of University and Research (MUR) under grant PRIN2022KB2HZM_002 "Finanziato dall'Unione Europea"—Next Generation EU and by the National Recovery and Resilience Plan (NRRP), Mission 04, Component 2, Investment 1.5—Next Generation EU, Call for tender no. 3277 dated 30 December 2021, award number: 0001052, dated 23 June 2022, project ECOSISTER.

Data Availability Statement: The original data presented in the study are openly available in AMSActa Institutional Research Repository at https://amsacta.unibo.it/id/eprint/8344 (accessed on 18 April 2025).

Conflicts of Interest: The authors declare no conflict of interest.

References

1. Hu, X.; Li, S.; Peng, H. A comparative study of equivalent circuit models for Li-ion batteries. *J. Power Sources* **2012**, *198*, 359–367. [CrossRef]
2. Van Haeverbeke, M.; Stock, M.; De Baets, B. Equivalent Electrical Circuits and Their Use Across Electrochemical Impedance Spectroscopy Application Domains. *IEEE Access* **2022**, *10*, 51363–51379. [CrossRef]
3. Meddings, N.; Heinrich, M.; Overney, F.; Lee, J.S.; Ruiz, V.; Napolitano, E.; Seitz, S.; Hinds, G.; Raccichini, R.; Gaberšček, M.; et al. Application of electrochemical impedance spectroscopy to commercial Li-ion cells: A review. *J. Power Sources* **2020**, *480*, 228742. [CrossRef]
4. Guha, A.; Patra, A. Online Estimation of the Electrochemical Impedance Spectrum and Remaining Useful Life of Lithium-Ion Batteries. *IEEE Trans. Instrum. Meas.* **2018**, *67*, 1836–1849. [CrossRef]
5. Zhang, Y.; Tang, Q.; Zhang, Y.; Wang, J.; Stimming, U.; Lee, A.A. Identifying degradation patterns of lithium ion batteries from impedance spectroscopy using machine learning. *Nat. Commun.* **2020**, *11*, 1706. [CrossRef]
6. Haussmann, P.; Melbert, J. Internal Cell Temperature Measurement and Thermal Modeling of Lithium Ion Cells for Automotive Applications by Means of Electrochemical Impedance Spectroscopy. *SAE Int. J. Altern. Powertrains* **2017**, *6*, 261–270. [CrossRef]
7. Liu, K.; Orfanoudakis, G.I.; Sharkh, S.M.; Cruden, A.J. Online Battery Pack Electrochemical Impedance Spectroscopy Measurement Using a Three-Phase Neutral Point Clamped Converter. In Proceedings of the 2023 International Conference on Clean Electrical Power (ICCEP), Terrasini, Italy, 27–29 June 2023; pp. 63–69. [CrossRef]
8. Koch, R.; Kuhn, R.; Zilberman, I.; Jossen, A. Electrochemical impedance spectroscopy for online battery monitoring—Power electronics control. In Proceedings of the 2014 16th European Conference on Power Electronics and Applications, Lappeenranta, Finland, 26–28 August 2014. [CrossRef]
9. Din, E.; Schaef, C.; Moffat, K.; Stauth, J.T. Online spectroscopic diagnostics implemented in an efficient battery management system. In Proceedings of the 2015 IEEE 16th Workshop on Control and Modeling for Power Electronics (COMPEL), Vancouver, BC, Canada, 12–15 July 2015. [CrossRef]
10. Crescentini, M.; De Angelis, A.; Ramilli, R.; De Angelis, G.; Tartagni, M.; Moschitta, A.; Andrea Traverso, P.; Carbone, P. Online EIS and Diagnostics on Lithium-Ion Batteries by Means of Low-Power Integrated Sensing and Parametric Modeling. *IEEE Trans. Instrum. Meas.* **2021**, *70*, 2001711. [CrossRef]
11. Fabozzi, M.; Ramilli, R.; Crescentini, M.; Traverso, P.A. A low-cost Electrochemical Impedance Spectroscopy-based sensor node for online battery cell monitoring. In Proceedings of the 2024 IEEE International Workshop on Metrology for Automotive (MetroAutomotive), Bologna, Italy, 26–28 June 2024; pp. 112–117. [CrossRef]
12. Teodorescu, R.; Sui, X.; Acharya, A.B.; Stroe, D.-I.; Huang, X. *Smart Battery Concept: A Battery That Can Breathe*; The Institution of Engineering and Technology: Stevenage, UK, 2022; pp. 214–220. [CrossRef]
13. Wei, Z.; Zhao, J.; He, H.; Ding, G.; Cui, H.; Liu, L. Future smart battery and management: Advanced sensing from external to embedded multi-dimensional measurement. *J. Power Sources* **2021**, *489*, 229462. [CrossRef]
14. Mattia, L.; Petrone, G.; Pirozzi, F.; Zamboni, W. A low-cost approach to on-board electrochemical impedance spectroscopy for a lithium-ion battery. *J. Energy Storage* **2024**, *81*, 110330. [CrossRef]
15. Ria, A.; Manfredini, G.; Gagliardi, F.; Vitelli, M.; Bruschi, P.; Piotto, M. Online High-Resolution EIS of Lithium-Ion Batteries by Means of Compact and Low Power ASIC. *Batteries* **2023**, *9*, 239. [CrossRef]

16. Locorotondo, E.; Cultrera, V.; Pugi, L.; Berzi, L.; Pierini, M.; Lutzemberger, G. Development of a battery real-time state of health diagnosis based on fast impedance measurements. *J. Energy Storage* **2021**, *38*, 102566. [CrossRef]
17. De Angelis, A.; Bertei, A.; Carbone, P. Characterization of Uncertainty in EIS and DRT Analysis of Lithium Batteries. In Proceedings of the 2024 IEEE International Workshop on Metrology for Automotive (MetroAutomotive), Bologna, Italy, 26–28 June 2024; pp. 106–111. [CrossRef]
18. Ramilli, R.; Santoni, F.; De Angelis, A.; Crescentini, M.; Carbone, P.; Traverso, P.A. Binary Sequences for Online Electrochemical Impedance Spectroscopy of Battery Cells. *IEEE Trans. Instrum. Meas.* **2022**, *71*, 2005208. [CrossRef]
19. Zappen, H.; Ringbeck, F.; Sauer, D. Application of Time-Resolved Multi-Sine Impedance Spectroscopy for Lithium-Ion Battery Characterization. *Batteries* **2018**, *4*, 64. [CrossRef]
20. Nian, H.; Li, M.; Hu, B.; Chen, L.; Xu, Y. Design Method of Multisine Signal for Broadband Impedance Measurement. *IEEE J. Emerg. Sel. Top. Power Electron.* **2022**, *10*, 2737–2747. [CrossRef]
21. Kallel, A.Y.; Kanoun, O. On the design of multisine signals for maintaining stability condition in impedance spectroscopy measurements of batteries. *J. Energy Storage* **2023**, *58*, 106267. [CrossRef]
22. Urquidi-Macdonald, M.; Real, S.; Macdonald, D.D. Applications of Kramers—Kronig transforms in the analysis of electrochemical impedance data—III. Stability and linearity. *Electrochim. Acta* **1990**, *35*, 1559–1566. [CrossRef]
23. Stolz, L.; Gaberšček, M.; Winter, M.; Kasnatscheew, J. Different Efforts but Similar Insights in Battery R&D: Electrochemical Impedance Spectroscopy vs Galvanostatic (Constant Current) Technique. *Chem. Mater.* **2022**, *34*, 10272–10278. [CrossRef]
24. Murbach, M.D.; Hu, V.W.; Schwartz, D.T. Nonlinear Electrochemical Impedance Spectroscopy of Lithium-Ion Batteries: Experimental Approach, Analysis, and Initial Findings. *J. Electrochem. Soc.* **2018**, *165*, A2758–A2765. [CrossRef]
25. Macdonald, J.R. Some new directions in impedance spectroscopy data analysis. *Electrochim. Acta* **1993**, *38*, 1883–1890. [CrossRef]
26. You, C.; Zabara, M.A.; Orazem, M.E.; Ulgut, B. Application of the Kramers–Kronig Relations to Multi-Sine Electrochemical Impedance Measurements. *J. Electrochem. Soc.* **2020**, *167*, 020515. [CrossRef]
27. Zhu, X.; Hallemans, N.; Wouters, B.; Claessens, R.; Lataire, J.; Hubin, A. Operando odd random phase electrochemical impedance spectroscopy as a promising tool for monitoring lithium-ion batteries during fast charging. *J. Power Sources* **2022**, *544*, 231852. [CrossRef]
28. Hallemans, N.; Widanage, W.D.; Zhu, X.; Moharana, S.; Rashid, M.; Hubin, A.; Lataire, J. Operando electrochemical impedance spectroscopy and its application to commercial Li-ion batteries. *J. Power Sources* **2022**, *547*, 232005. [CrossRef]
29. Hallemans, N.; Howey, D.; Battistel, A.; Saniee, N.F.; Scarpioni, F.; Wouters, B.; La Mantia, F.; Hubin, A.; Widanage, W.D.; Lataire, J. Electrochemical impedance spectroscopy beyond linearity and stationarity—A critical review. *Electrochim. Acta* **2023**, *466*, 142939. [CrossRef]
30. Schroeder, M.R. Synthesis of Low-Peak-Factor Signals and Binary Sequences with Low Autocorrelation. *IEEE Trans. Inf. Theory* **1970**, *16*, 85–89. [CrossRef]
31. Van Der Ouderaa, E.; Schoukens, J.; Renneboog, J. Peak Factor Minimization of Input and Output Signals of Linear Systems. *IEEE Trans. Instrum. Meas.* **1988**, *37*, 207–212. [CrossRef]
32. Yang, Y.; Zhang, F.; Tao, K.; Sanchez, B.; Wen, H.; Teng, Z. An improved crest factor minimization algorithm to synthesize multisines with arbitrary spectrum. *Physiol. Meas.* **2015**, *36*, 895. [CrossRef] [PubMed]
33. Guillaume, P.; Schoukens, J.; Pintelon, R.; Kollar, I. Crest-Factor Minimization Using Nonlinear Cheby shev Approximation Methods. *IEEE Trans. Instrum. Meas.* **1991**, *40*, 982–989. [CrossRef]
34. Retzler, A.; Cseppentő, B.; Swevers, J.; Gillis, J.; Leitold, L.; Kollár, Z. Improved crest factor minimization of multisine excitation signals using nonlinear optimization. *Automatica* **2022**, *146*, 110654. [CrossRef]
35. Ojarand, J.; Min, M. Recent Advances in Crest Factor Minimization of Multisine. *Elektron. Elektrotechnika* **2017**, *23*, 59–62. [CrossRef]
36. Horner, A.; Beauchamp, J. A genetic algorithm-based method for synthesis of low peak amplitude signals. *J. Acoust. Soc. Am.* **1996**, *99*, 433–443. [CrossRef]
37. Hu, Y.; Ramos, P.M.; Janeiro, F.M. Artificial bee colony algorithm for peak-to-peak factor minimization in periodic signals. In Proceedings of the 22nd IMEKO TC4 International Symposium & 20th International Workshop on ADC Modelling and Testing Supporting World Development Through Electrical & Electronic Measurements, Iasi, Romania, 14–15 September 2017; pp. 271–274.
38. Kallel, A.Y.; Kanoun, O. Crest Factor Optimization for Multisine Excitation Signals with Logarithmic Frequency Distribution Based on a Hybrid Stochastic-Deterministic Optimization Algorithm. *Batteries* **2022**, *8*, 176. [CrossRef]
39. Kallel, A.Y.; Bouchaala, D.; Kanoun, O.; Kallel, A.Y.; Bouchaala, D.; Kanoun, O. Critical implementation issues of excitation signals for embedded wearable bioimpedance spectroscopy systems with limited resources. *MeScT* **2021**, *32*, 084011. [CrossRef]
40. Luciani, G.; Ramilli, R.; Romani, A.; Tartagni, M.; Traverso, P.A.; Crescentini, M. A miniaturized low-power vector impedance analyser for accurate multi-parameter measurement. *Measurement* **2019**, *144*, 388–401. [CrossRef]

41. Lowenthal, N.; Ramilli, R.; Crescentini, M.; Traverso, P.A. Development of a numerical framework for the analysis of a multi-tone EIS measurement system. In Proceedings of the 2023 IEEE International Workshop on Metrology for Automotive (MetroAutomotive), Modena, Italy, 28–30 June 2023; pp. 41–45. [CrossRef]
42. De Angelis, A.; Ramilli, R.; Crescentini, M.; Moschitta, A.; Carbone, P.; Traverso, P.A. In-Situ Electrochemical Impedance Spectroscopy of Battery Cells by Means of Binary Sequences. In Proceedings of the 2021 IEEE International Instrumentation and Measurement Technology Conference (I2MTC), Glasgow, UK, 17–20 May 2021; pp. 1–5.
43. Howey, D.A.; Mitcheson, P.D.; Yufit, V.; Offer, G.J.; Brandon, N.P. Online measurement of battery impedance using motor controller excitation. *IEEE Trans. Veh. Technol.* **2014**, *63*, 2557–2566. [CrossRef]
44. Wikner, E.; Lesser, J. Accelerated lithium-ion battery cycle lifetime testing by condition-based reference performance tests. *Meas. Energy* **2024**, *4*, 100019. [CrossRef]
45. Dubarry, M.; Baure, G. Perspective on Commercial Li-ion Battery Testing, Best Practices for Simple and Effective Protocols. *Electronics* **2020**, *9*, 152. [CrossRef]
46. Marelli Unveils Latest Innovative Battery Management Systems Solution at CTI Symposium Berlin. 2024. Available online: https://www.marelli.com/en/news/marelli-unveils-latest-innovative-battery-management-systems-sol.html (accessed on 18 April 2025).
47. Battery Cell Management Unit (CMU)—Sensichips—Learning MICROSENSORS. Available online: https://sensichips.com/battery-cell-management-unit/ (accessed on 18 April 2025).